Applications of Multigrid Methods for the Simulation of Non-Newtonian Fluid Flows

Young Ju Lee

leeyoung@math.rutgers.edu

supported by NSF

Department of Mathematics
Rutgers University

NIA, Hampton, VA, Aug 21, 2012

Outline of the Talk

- Introduction
  1. Model Equations and Full Discretizations
  2. Some Numerical Experiments for Modeling Physical Phenomena
- Difficulties in Simulating Non-Newtonian Fluids and Their remedies
  1. Boundary Condition for Stabilized Models
  2. Parallel Solvers for Stokes Equation in 2D and 3D.
  3. Uniformly Accurate FEM for Stokes-Like Equations
  4. Multigrid-Based Fast and Robust Methods for Stokes-Like Equations
- Further Enhancement in Progress
  1. GPU computing.

Stokes Equations

$$
\begin{aligned}
-\Delta \mathbf{u} + \nabla p &= \mathbf{f} \\
\nabla \cdot \mathbf{u} &= 0
\end{aligned}
$$

Navier-Stokes Equations

$$\begin{aligned} \mathrm{Re}\frac{D\mathbf{u}}{Dt} - \Delta\mathbf{u} + \nabla p &= \mathbf{f} \\ \nabla\cdot\mathbf{u} &= 0, \end{aligned}$$

where

$$\frac{D\mathbf{u}}{Dt} = \frac{\partial\mathbf{u}}{\partial t} + \mathbf{u}\cdot\nabla\mathbf{u}.$$

Remark : Nonlinearity is hidden in the material derivative.

Non-Newtonian Equations

$$
\begin{aligned}
\mathrm{Re}\frac{D\mathbf{u}}{Dt} - \mu_s \Delta \mathbf{u} + \nabla p &= \mu_p \nabla \cdot \boldsymbol{\tau} + \mathbf{g} \\
\nabla \cdot \mathbf{u} &= 0, \\
\frac{D\boldsymbol{\tau}}{Dt} - \nabla \mathbf{u}\, \boldsymbol{\tau} - \boldsymbol{\tau}\, (\nabla \mathbf{u})^T &= \frac{1}{\mathrm{Wi}}(\boldsymbol{\delta} - \boldsymbol{\tau}),
\end{aligned}
$$

where

$$
\frac{D\mathbf{u}}{Dt} = \frac{\partial \mathbf{u}}{\partial t} + \mathbf{u} \cdot \nabla \mathbf{u} \quad \text{and} \quad \frac{D\boldsymbol{\tau}}{Dt} = \frac{\partial \boldsymbol{\tau}}{\partial t} + \mathbf{u} \cdot \nabla \boldsymbol{\tau}.
$$

1. Parameter Wi (≥ 0) denotes the measure of elasticity that makes the underlying fluids to differ from the Newtonian fluids.
2. The instability can occur for relatively large Weissenberg number even for vanishingly small Reynolds number, Re.

Semi-Discrete Equation for Momentum equations

Semi-Lagrangian Scheme: Pironneau and Douglas and Russell (80')

$$\begin{aligned} \frac{D\mathbf{u}(x,t)}{Dt} &= \frac{\partial \mathbf{u}(x,t)}{\partial t} + \mathbf{u}(x,t)\cdot\nabla\mathbf{u}(x,t) \\ &\approx \frac{\mathbf{u}(x,t)-\mathbf{u}(x^*,t-h_t)}{h_t}, \end{aligned}$$

where x is generally, the spatial node or computational quadrature points and x^* is the solution to the ODE

$$\frac{dy}{dt} = u(y,t), \quad \text{where } y(t) = x. \tag{1}$$

Remark : Problems such as numerical errors and instability may occur in the evaluation of quantity relevant to $\mathbf{u}(x^*, t-h_t)$.

Semi-Discrete Equation I for Constitutive Equations

$$\begin{aligned}\frac{D\tau(x,t)}{Dt} &= \frac{\partial\tau(x,t)}{\partial t} + \mathbf{u}(x,t)\cdot\nabla\tau(x,t)\\ &\approx \frac{\tau(x,t)-\tau(x^*,t-h_t)}{h_t}.\end{aligned}$$

The use of the semi-Lagrangian discretization leads to the semi-discrete constitutive equation :

$$A\tau + \tau A^T = C,$$

where

$$A = \frac{1}{2}\left(\frac{1}{\mathrm{Wi}} + \frac{1}{h_t}\right)\boldsymbol{\delta} - \nabla\mathbf{u} \quad \text{and} \quad C = \frac{1}{\mathrm{Wi}}\boldsymbol{\delta} + \frac{1}{h_t}\tau(x^*, t-h_t).$$

Remark: The semi-discrete Constitutive equation becomes Algebraic Riccati Equations.

Semi-Discrete Equation II for Constitutive Equations

Definition (Lie Derivative)

We define the Lie derivative of a symmetric tensor ζ in the Eulerian frame as: for $t, s \geq 0$,

$$\frac{D\zeta}{Dt} - \nabla \mathbf{u}\, \zeta - \zeta\, (\nabla \mathbf{u})^T := \mathsf{F}(t,s) \frac{\partial \left(\mathsf{F}(s,t) \zeta(s) \mathsf{F}(s,t)^T \right)}{\partial s} \mathsf{F}(t,s)^T \Big|_{s=t}, \quad (2)$$

where $\mathsf{F}(t,s)$ is the deformation gradient defined by

$$\frac{\partial \mathsf{F}(t,s)}{\partial s} = \nabla \mathbf{u}(t,s) \mathsf{F}(t,s) \quad \text{and} \quad \mathsf{F}(t,t) = \boldsymbol{\delta}. \quad (3)$$

The semi-discrete constitutive equation reads :

$$\frac{1}{h_t} \left(\boldsymbol{\tau}^{n+1} - \mathsf{F} \boldsymbol{\tau}^n (x^*, s) \mathsf{F}^T \right) = \frac{1}{\mathrm{Wi}} (\boldsymbol{\delta} - \tau^{n+1}), \quad (4)$$

Fully Discrete Equations : Non-Newtonian Equations

$$
\begin{aligned}
\mathrm{Re} D_t^h \mathbf{u}_h^{n+1} - \mu_s \Delta_h \mathbf{u}_h^{n+1} + \nabla_h p_h^{n+1} &= \mu_p \widetilde{\nabla}_h \cdot \boldsymbol{\tau}_h^{n+1} + \mathbf{g} \\
\nabla_h \cdot \mathbf{u}_h^{n+1} &= 0, \\
\left(1 + \frac{h_t}{\mathrm{Wi}}\right) \boldsymbol{\tau}_h^{n+1} &= \frac{1}{\mathrm{Wi}} \boldsymbol{\delta} + \mathrm{F}_h \boldsymbol{\tau}^n(x^*, s) \mathrm{F}_h^T,
\end{aligned}
$$

where

$$
\mathrm{F}_h = \left(\boldsymbol{\delta} - h_t \widetilde{\nabla}_h \mathbf{u}_h^{n+1}\right)^{-1}. \tag{5}
$$

Remark : The discrete differential operators can be from finite difference, finite elements etc.

Fully Discrete Equations : How to handle these equations ?

$$
\begin{aligned}
\mathrm{Re} D_t^h \mathbf{u}_h^{n+1} - \mu_s \Delta_h \mathbf{u}_h^{n+1} + \nabla_h p_h^{n+1} &= \mu_p \widetilde{\nabla}_h \cdot \boldsymbol{\tau}_h^{n+1} + \mathbf{g} \\
\nabla_h \cdot \mathbf{u}_h^{n+1} &= 0, \\
\left(1 + \frac{h_t}{\mathrm{Wi}}\right) \boldsymbol{\tau}_h^{n+1}(x,t) &= \frac{1}{\mathrm{Wi}} \boldsymbol{\delta} + \mathrm{F}_h \boldsymbol{\tau}^n(x^*, s) \mathrm{F}_h^T,
\end{aligned}
$$

where $\mathrm{F}_h = \left(\boldsymbol{\delta} - h_t \widetilde{\nabla}_h \mathbf{u}_h^{n+1}\right)^{-1}$.

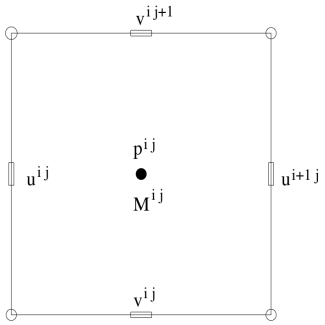

- Nonlinear iteration should be used.
- Fast Solution method is required for the Stokes-Like equations for the fast solution to the non-Newtonian equations.

Instability in Highly Elastic Flows

The onset of the instability at high Weissenberg number regime for the Oldroyd-B model. Flow becomes unsteady at some critical Weissenberg number.

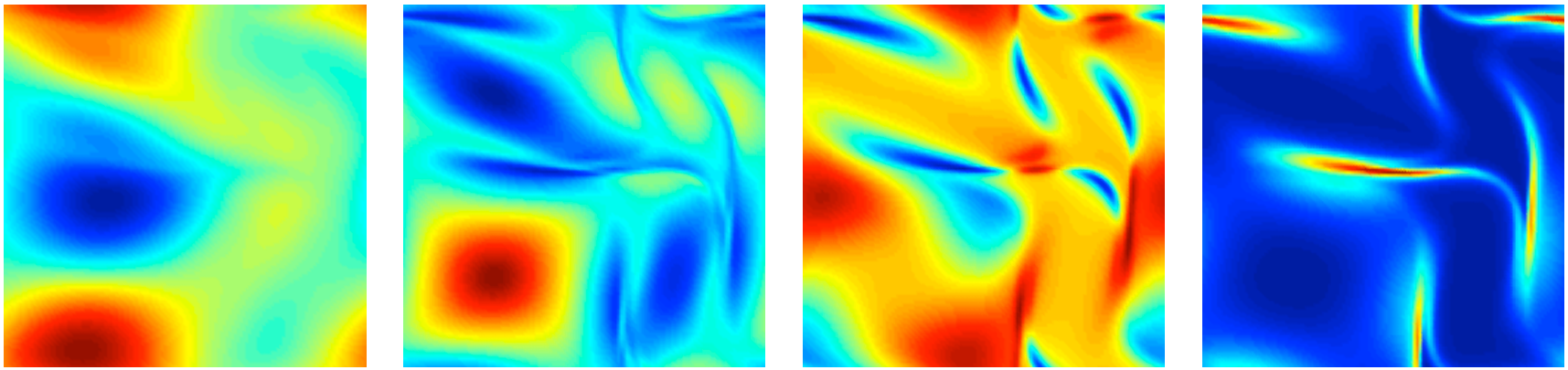

Figure: Ux $\in$ [-0.4,0.4], Vorticity $\in [-0.5, 0.8]$, $\boldsymbol{\tau}_{xy} \in [-50, 25]$, $\mathrm{tr}\boldsymbol{\tau} \in [0, 380]$ at $t = 480$ from Left to Right, Lee (Preprint, 2011). Results of OB model ($\epsilon = 0$) in the four roll mill geometry with Wi $= 10$. External force is $\mathbf{g} = (-2\sin x \cos y, 2\cos x \sin y)$ and initial condition is (Becca and Shelley, PRL (2009)) – IDEA came from Brandt and Boris

$$\boldsymbol{\tau}(\mathbf{x}, 0) = \boldsymbol{\delta} + \begin{pmatrix} \varepsilon_1 g(x)\cos(y) & -\varepsilon_2 \sin(x)\cos(y) \\ -\varepsilon_2 \sin(x)\cos(2y) & \varepsilon_3 \cos(x) g(y) \end{pmatrix}.$$

Instability in Highly Elastic Flows

The onset of the instability at high Weissenberg number regime for the Oldroyd-B model. Flow becomes unsteady at some critical Weissenberg number.

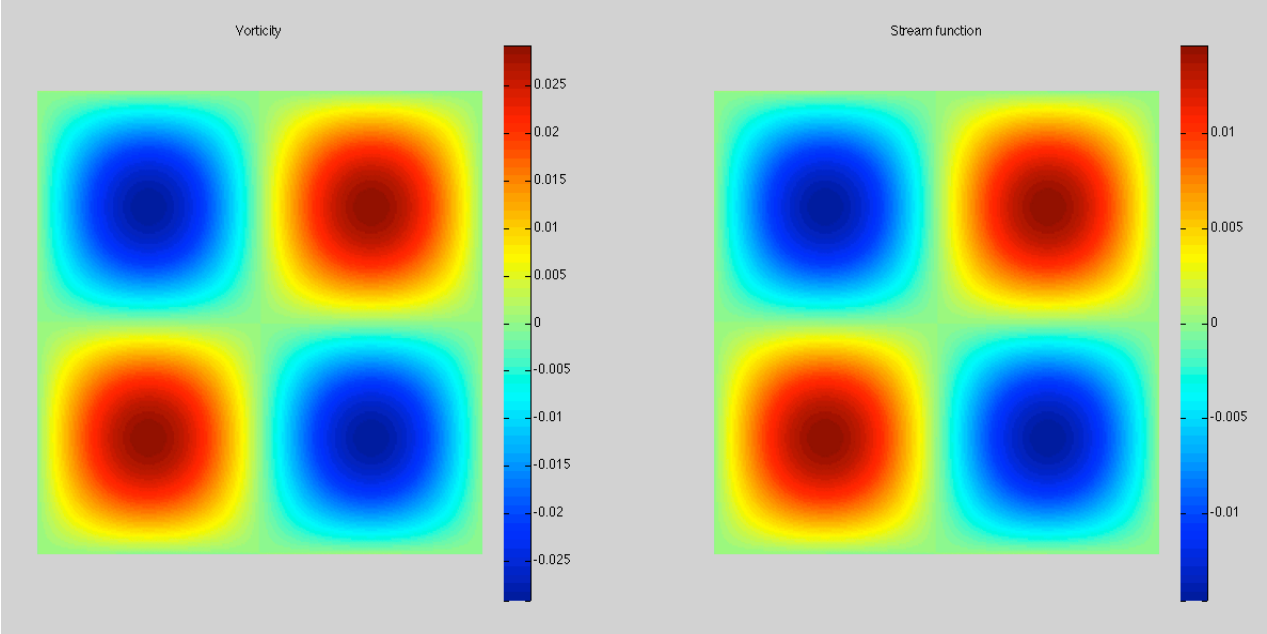

Figure: Vorticity and Stream function for Newtonian flows at Re = 1000 at time level 1. – IDEA came from Brandt and Boris

Falling Ball in Wormlike Micellar Fluids

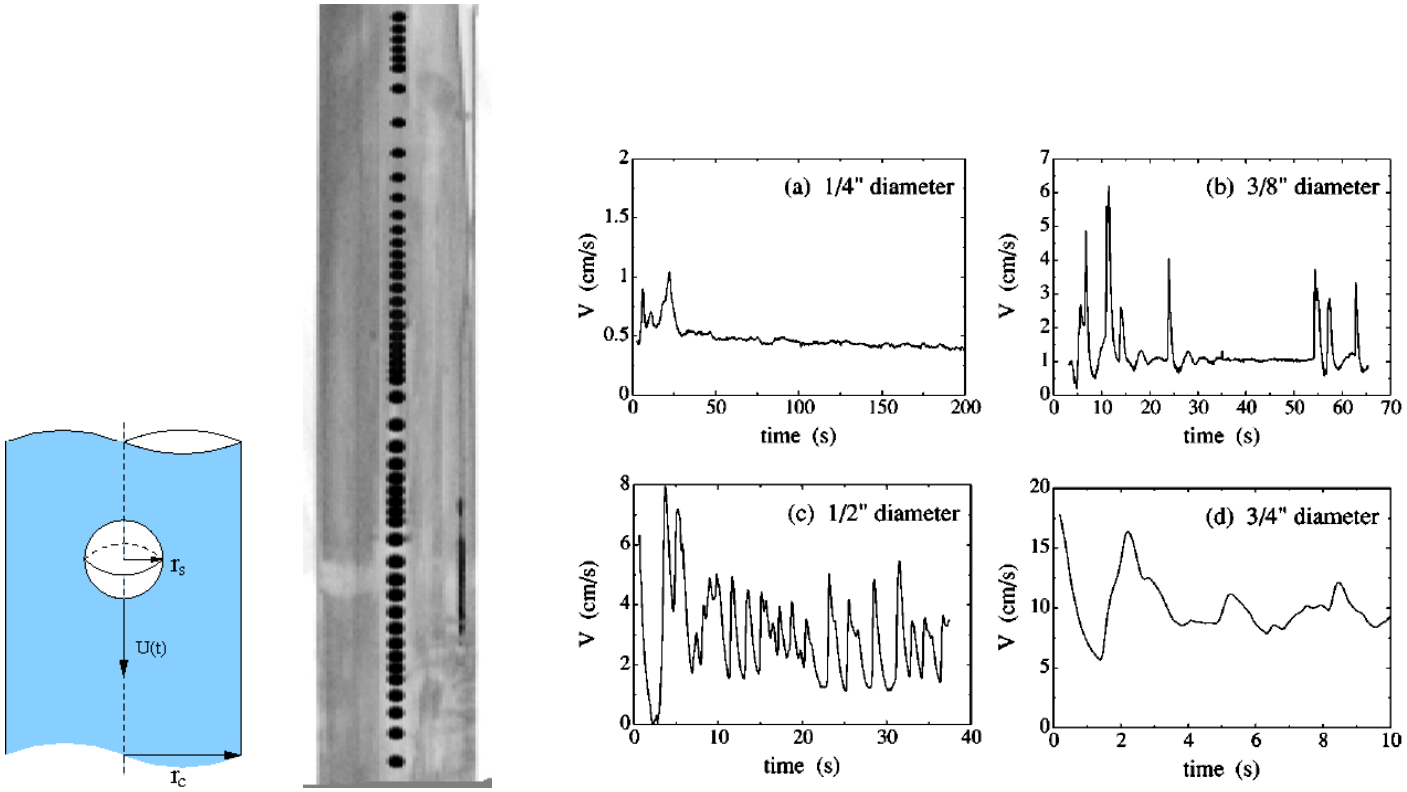

(a) Domain (b) Image (c) Speed v.s. Time

Figure: Experimental Results obtained by A. Jayaraman and A. Belmonte 2003.

Simulation of the Falling Sphere - with C. Zhang

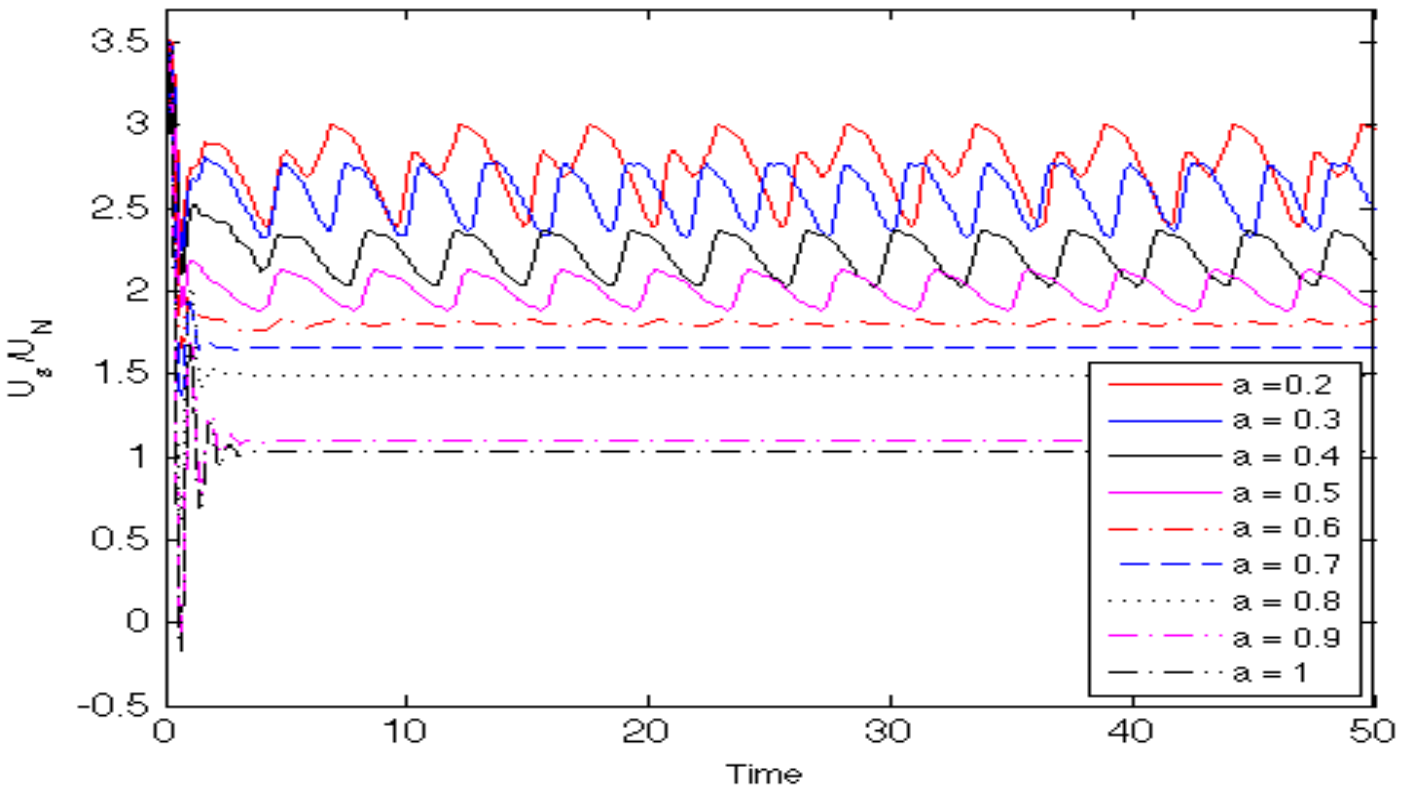

Figure: The nominal speed of the falling sphere as a function of ξ.

Difficulties in Simulating Non-Newtonian Fluids

1. There is a stability issue at high Weissenberg number regime.
2. FEM-formulation is done using Hood-Taylor mixed elements for which there is still a room to be improved in the efficiency of the Stokes solver.
3. Local solvers for the conformation tensor can be enhanced by employing the parallel technique.

High-Weissenberg Number Problem : Benchmark Oldroyd-B Flow

Simulations with C. Zhang and J. Xu (Handbook of Numerical Analysis (2011))

Wi/Drag	Kufperman et. al. (2006)	Lee, Zhang and Xu (2010)
0.1	132	129
0.3	123	121
0.5	118	117
0.7	117	116
1.0	119	121
1.5	125	142
2.0	135	179

1. There is certainly a problem in stability at High Weissenberg number regime such as the blow-up for relatively large time step sizes.
2. The loss of reliability for numerical solutions at High Weissenberg number regime is mainly due to the lack of the mesh convergence.

Non-Newtonian Equation - Stabilized Oldroyd-B Model

$$\mathrm{Re}\frac{D\mathbf{u}}{Dt} - \mu_s \Delta \mathbf{u} + \nabla p = \nabla \cdot \mathcal{S}_\alpha(\boldsymbol{\tau}) + \mathbf{g}, \qquad \nabla \cdot \mathbf{u} = 0,$$

$$\boldsymbol{\tau} + \mathrm{Wi}\left(\frac{D\boldsymbol{\tau}}{Dt} - \nabla \mathcal{S}_\alpha(\mathbf{u})\,\boldsymbol{\tau} - \boldsymbol{\tau}\left(\nabla \mathcal{S}_\alpha(\mathbf{u})\right)^T\right) - \varepsilon^2 \Delta \boldsymbol{\tau} = \frac{1-\mu_s}{\mathrm{Wi}}\boldsymbol{\delta},$$

Strategy : Change the model (E. Suli and J. Barrett (2007))

(1) Adding the Diffusion

(2) Mollifying the velocity fields (Leray-α model)

Remark

- *The physical diffusion coefficient is in fact present in the range of $\varepsilon^2 = 10^{-7} - 10^{-9}$ for the domain of $1\mathrm{cm}$ scale. The importance of the diffusion increases for small scale problems.*
- *The introduction of the mollifier, $\mathcal{S}_\alpha$ makes the system globally well-posed even without the diffusion - Suli and Barrett (2007).*

Rheology of Stabilized Oldroyd-B Model and Original Oldroyd-B Model

Theorem (Li and Lee (2010))

Under the assumption that the flow is periodic or the stress fields satisfy the pure Neumann condition, the solution to the Stabilized Oldroyd-B model approaches to that of the Original Oldrody-B model.

Remark

- *The rheology of the Stabilized model can be close to that of the Original model when* $\varepsilon^2 \ll 1$ *at least in the interior.*
- *The rheology may be different near the boundary, for the numerical solution by employing the pure Neumann boundary condition.*

Some Boundary Conditions for Diffusive Oldroyd-B Model

1. Pure Neumann Boundary Condition $\nabla \boldsymbol{\tau} \cdot \mathbf{n} = 0$ is used by Graham et al. (2001) and also E. Suli and J. Barrett (2007).
2. Robin Boundary Condition is attempted by P. Olmsted recently (2009)
3. The Dirichlet boundary condition is used by Sureshkumar and Beris (1995), will be clarified shortly.

New Boundary Condition (Li and Lee) (2010)

The dumbbell model can be driven from the following two SDEs

$$dr_t = \mathbf{u}(r_t)dt + \sqrt{\frac{4k\mathrm{T}}{\zeta}}dW_t^r \tag{6}$$

$$dQ_t = \left[Q_t \cdot \nabla\mathcal{S}_\alpha(\mathbf{u}) - \frac{2}{\zeta}\frac{\partial\phi}{\partial Q_t}\right]dt + \sqrt{\frac{4k\mathrm{T}}{\zeta}}dW_t^Q. \tag{7}$$

ϕ is a potential, Q_t is end-to-end vector of bead-spring and r_t is the center of mass. Replace the equation (6) at the boundary into :

$$dr_t = \mathbf{u}(r_t)dt + \varepsilon\sqrt{\frac{2}{\mathrm{Wi}}}\mu \cdot dW_t^r\mu, \quad \text{where } \mu = \mathbf{u}/|\mathbf{u}|. \tag{8}$$

The continuum equation at the boundary becomes :

$$\frac{D\boldsymbol{\tau}}{Dt} - (\nabla\mathcal{S}_\alpha(\mathbf{u}))\boldsymbol{\tau} - \boldsymbol{\tau}(\nabla\mathcal{S}_\alpha(\mathbf{u}))^T = \varepsilon^2\frac{1}{\mathrm{Wi}}(\mu\cdot\nabla)^2\boldsymbol{\tau} + \frac{1}{\mathrm{Wi}}(\boldsymbol{\delta} - \boldsymbol{\tau}).$$

Numerical Experiment I (Li and Lee) (2010)

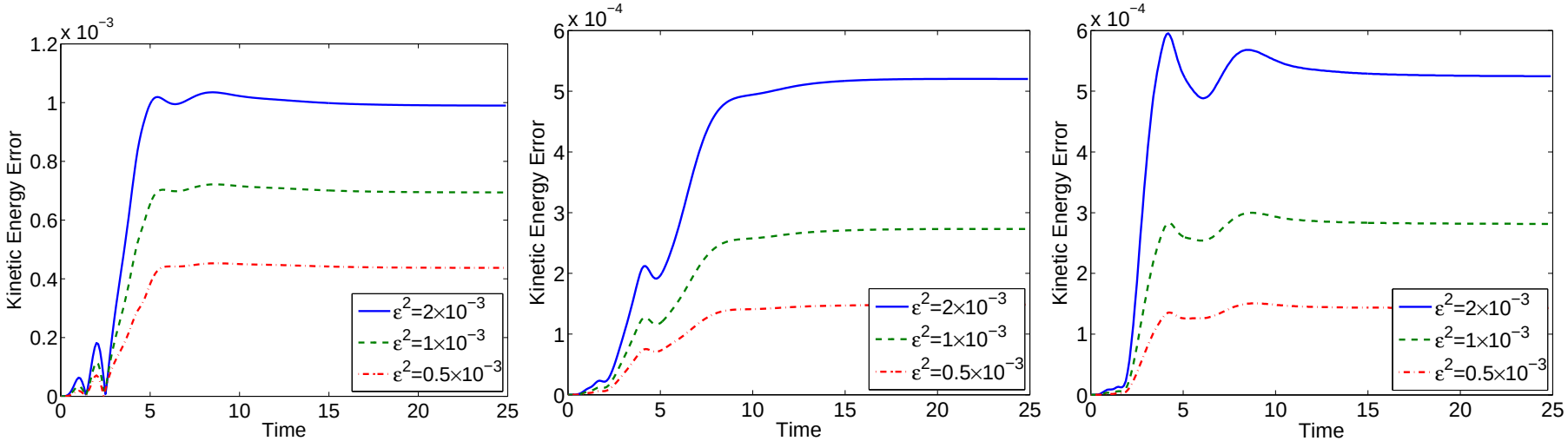

Figure: The results of the kinetic energy error in the simulation for the Lid-driven cavity flow of the Oldroyd-B model with Wi $= 2$. (Left), (Middle) and (Right) correspond to the results from the pure Neumann boundary condition $\mathcal{N}$ and the Dirichlet boundary condition $\mathcal{D}_{\mathbf{0}}$, $\mathcal{D}_{\varepsilon}$, respectively. The convergence rate is $O(\varepsilon^2)$ for $\mathcal{D}_{\mathbf{0}}$ and $\mathcal{D}_{\varepsilon}$.

Numerical Experiment II (Li and Lee) (2010)

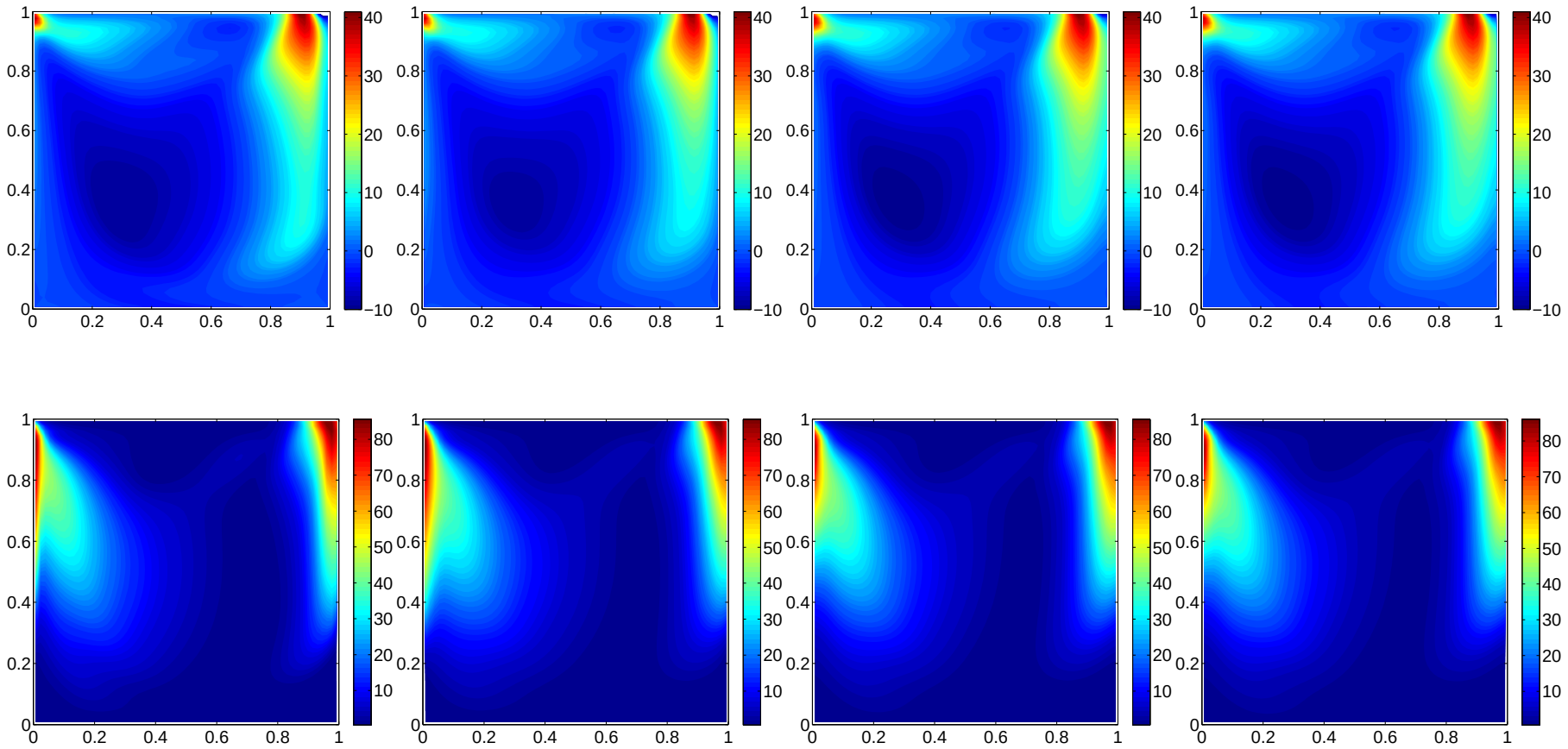

Figure: Plots of τ_{xy} (1st row) and τ_{yy} (2nd row) for Lid-driven cavity flow at $t = 25$ with $\mathrm{Wi} = 5$. The first column is the solution from the non-Diffusive FENE-CR and the second, third and fourth columns are solutions from the Diffusive model with $\varepsilon^2 = 0.001$ and BCs, $\mathcal{D}_\varepsilon, \mathcal{D}_0$ and $\mathcal{N}$

Numerical Experiment III (Li and Lee) (2010)

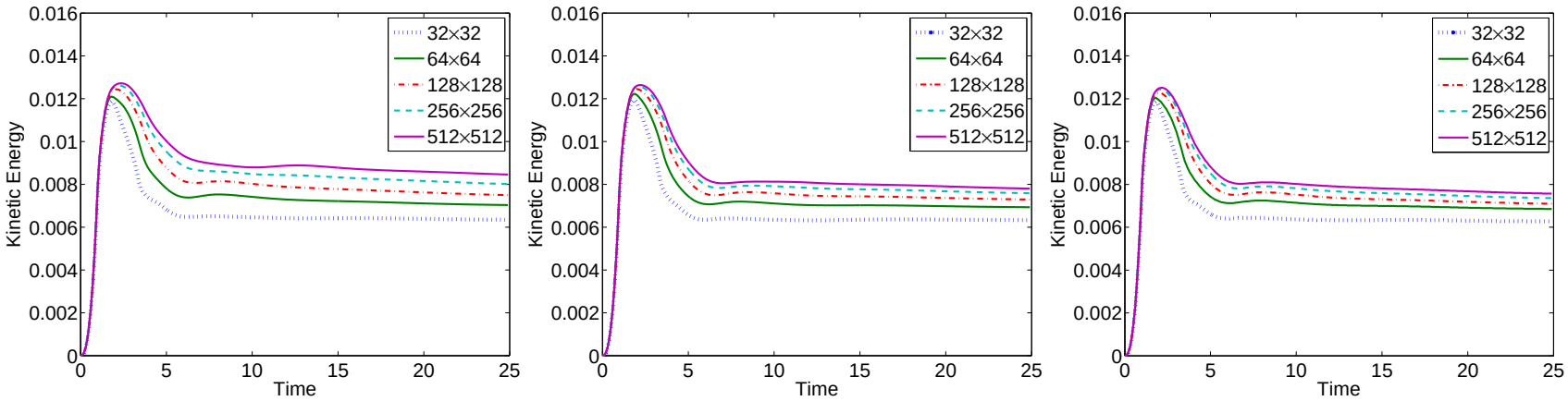

Figure: The result of kinetic energy for Wi $= 5$ of the FENE-CR. (Left) is for non-Diffusive model. (Middle) and (Right) are the diffusive models with $\varepsilon^2 = 0.001$ and BCs, $\boldsymbol{\mathcal{D}}_0$ and $\boldsymbol{\mathcal{D}}_\varepsilon$, respectively.

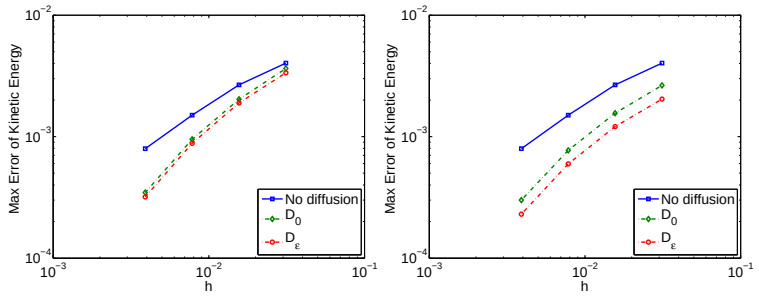

Figure: The result of mesh convergence rate for non-Diffusive and Diffusive model with BCs, $\boldsymbol{\mathcal{D}}_0$ and $\boldsymbol{\mathcal{D}}_\varepsilon$ with $\varepsilon^2 = 0.001$ (Left) and $\varepsilon^2 = 0.01$ (Right).

Difficulties in Simulating Non-Newtonian Fluids

1. There is a stability issue at high Weissenberg number regime.
2. FEM-formulation is done using Hood-Taylor mixed elements for which there is still a room to be improved in the efficiency of the Stokes solver.
3. Local solvers for the conformation tensor can be enhanced by employing the parallel technique.

Preconditioned MINRes used for Stokes Eq based on FEM

The operator form of the problem is given as follows:

$$\begin{pmatrix} \rho^2 I - \kappa^2 \Delta_h & \nabla_h \\ -\mathrm{div}_h & 0 \end{pmatrix} \begin{pmatrix} \mathbf{u}_h \\ p_h \end{pmatrix} = \begin{pmatrix} \mathbf{f}_h \\ 0 \end{pmatrix}.$$

The preconditioner can be chosen to be of the block diagonal form :

$$\begin{pmatrix} \left(\rho^2 I - \kappa^2 \Delta_h\right)^{-1} & 0 \\ 0 & \frac{\kappa^2}{\rho^2} I + (-\Delta_h)_N^{-1} \end{pmatrix}$$

Preconditioned MINRes used for Stokes Eq based on FEM

Parallel Preconditioned MINRES with Hypre AMG preconditioner for blocks with the relative residual $< 10^{-6}$. (2D results)

DOF	36,483	146,491	588,291	2,356,227
# of iterations	39	39	35	33

Remark There is a room for improvement !

Auxiliary Space Preconditioner for Poisson Eq (3D)

- AMG (Hypre) methods for poisson equation on linear finite element.
- Transfer operator between $P^{k,0}$ and $P^{1,0}$.
- Smoother for poisson equation on the $P^{k,0}$ element for $k \geq 1$. (PHG)

Method	1 Core			8 Cores			64 Cores		
	#It	CPU	RAM	#It	CPU	RAM	#It	CPU	RAM
AMG(0.2)	15	36.95	1241	21	48.11	1095	153	155.9	1003
GAMG(0.2)	16	7.95	901	18	8.50	783	18	8.61	738
AMG(0.4)	17	16.93	1042	35	32.27	895	>500	>300	836
GAMG(0.4)	16	7.97	902	18	8.45	783	18	9.41	738
AMG(0.6)	18	11.19	908	19	14.98	772	49	35.19	734
GAMG(0.6)	16	7.98	902	18	8.39	783	18	8.99	738
AMG(0.8)	18	8.64	848	18	11.09	719	18	12.91	672
GAMG(0.8)	16	7.96	899	18	8.35	783	18	8.71	737

Table: Comparison of preconditioners for the 3D Poisson's equation with about 460K DOF per processing core (P^4 finite element method).

Auxiliary Space Preconditioner for Poisson Eq (3D)

Let $\Omega \subset \mathbb{R}^d$ be a bounded polygonal domain. We consider the Poisson equation subject to zero Dirichlet condition on $\partial\Omega$. Find $u \in H_0^1(\Omega)$ such that

$$a(u, v) = \langle f, v \rangle, \quad \forall v \in H_0^1(\Omega),$$

where $a(u, v) = \int_\Omega \nabla u \cdot \nabla v \, dx$ and $\langle f, v \rangle = \int_\Omega fv \, dx$.

$$\begin{aligned} V_h^k &= \{v \in C(\Omega) : v|_T \in P^k(T), \forall T \in \mathcal{T}_h\} = \mathrm{span}\{\phi_1, \cdots, \phi_{n_h}\} \\ V_H &= V_h^1 = \mathrm{span}\{\psi_1, \cdots, \psi_{n_H}\}. \end{aligned}$$

Note that

$$\psi_j = \sum_{i \in N_h^H(j)} \psi_j(x_i^h)\phi_i, N_h^H(j) = \{i \in \{1, \cdots, n_h\} : \mathrm{supp}(\phi_i) \cap \mathrm{supp}(\psi_j) \neq \emptyset\}.$$

The transfer operators are then with $\psi_j(x_i^h) = \mathbf{c}_j^i$.

$$\mathsf{I}_\mathsf{P} = (\mathbf{c}_1 \cdots \mathbf{c}_{n_H}) \in \mathbb{R}^{n_h \times n_H} \quad \text{and} \quad \mathsf{I}_\mathsf{R} = \mathsf{I}_\mathsf{P}^T.$$

Auxiliary Space Preconditioner for Poisson Eq (GAMG)

Set

$$v_h = \sum_{i=1}^{n_H} \overline{v}_i \psi_i + \sum_{i=1}^{n_h} \widehat{v}_i \phi_i.$$

Let $\widetilde{V}_h = \mathrm{span}\{\psi_1, \cdots, \psi_{n_H}, \phi_1, \cdots, \phi_{n_h}\}$ and find v_h such that

$$a(v_h, w_h) = \langle f, w_h \rangle, \quad \forall w_h \in \widetilde{V}_h.$$

This leads to the following augmented matrix system :

$$\mathcal{A} \begin{pmatrix} \overline{v} \\ \widehat{v} \end{pmatrix} = \widetilde{f} \quad \text{with } \mathcal{A} = \begin{pmatrix} \mathsf{I}_\mathsf{R} A_h \mathsf{I}_\mathsf{P} & \mathsf{I}_\mathsf{R} A_h \\ A_h \mathsf{I}_\mathsf{P} & A_h \end{pmatrix}, \widetilde{f} = \begin{pmatrix} \mathsf{I}_\mathsf{R} f_h \\ f_h \end{pmatrix}$$

Auxiliary Space Preconditioner for Poisson Eq (GAMG)

Theorem

GAMG is equivalent to GS for the augmented system. The convergence rate is given by

$$|I - (\mathcal{D} - \mathcal{L})^{-1}\mathcal{A}|_{\mathcal{A}}^2 = 1 - \frac{1}{K},$$

where

$$K = 1 + \sup_{\widetilde{u} \in \mathcal{N}^{\perp}} \inf_{\widetilde{c} \in \mathcal{N}} \frac{(\mathcal{L}\mathcal{D}^{-1}\mathcal{L}^T(\widetilde{u} + \widetilde{c}), (\widetilde{u} + \widetilde{c}))}{(\widetilde{u}, \widetilde{u})_{\mathcal{A}}} \lesssim \sup_{v_h \in V_h} \frac{\|v_h - Q_H v_h\|_1}{\|v_h\|_1} + 1.$$

Auxiliary Space Preconditioner for Poisson Eq (3D)

Element Type	$\theta = 0.2$	$\theta = 0.4$	$\theta = 0.6$	$\theta = 0.8$
$P^{2,0}$	5.0	3.0	2.2	2.0
$P^{3,0}$	6.7	3.8	2.4	1.9
$P^{4,0}$	18.0	32.0	4.0	1.5

Table: Speedup of GAMG preconditioner compared with AMG preconditioner for solving the Poisson equation on unstructured tetrahedron mesh with 64 cores (about 10 million degrees of freedom).

- The AMG method performs very well even for high-order finite element methods.
- The AMG method is sensitive to the strength threshold θ; and, it is even more so for higher order element.
- The GAMG method works better than AMG and it is very robust with respect to θ.
- The GAMG method requires similar amount of RAM as the AMG method.

Auxiliary Space Preconditioner for Poisson Eq (3D)

Parallel (weak) scalability of AMG and GAMG for P3 (Top) and P4 (Bottom) Poisson Eqs

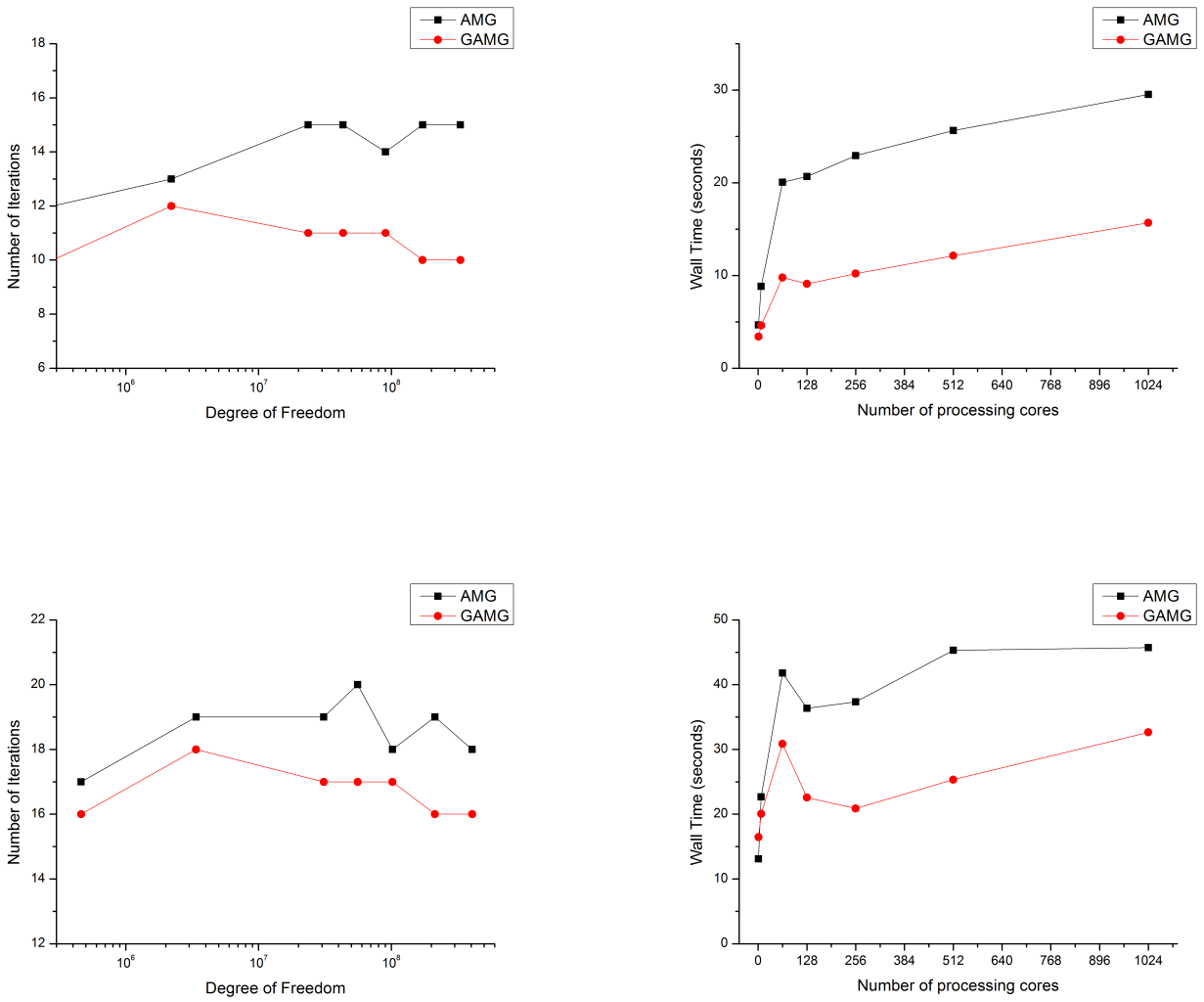

Auxiliary Space Preconditioner for Hood-Taylor Stokes Eqs

- GAMG methods for higher-order poisson equation.
- GMRes solver in PETSc.

Parallel (weak) scalability of Preconditioned Stokes Eqs : P3-P2 (Top), P4-P3 (Bottom)

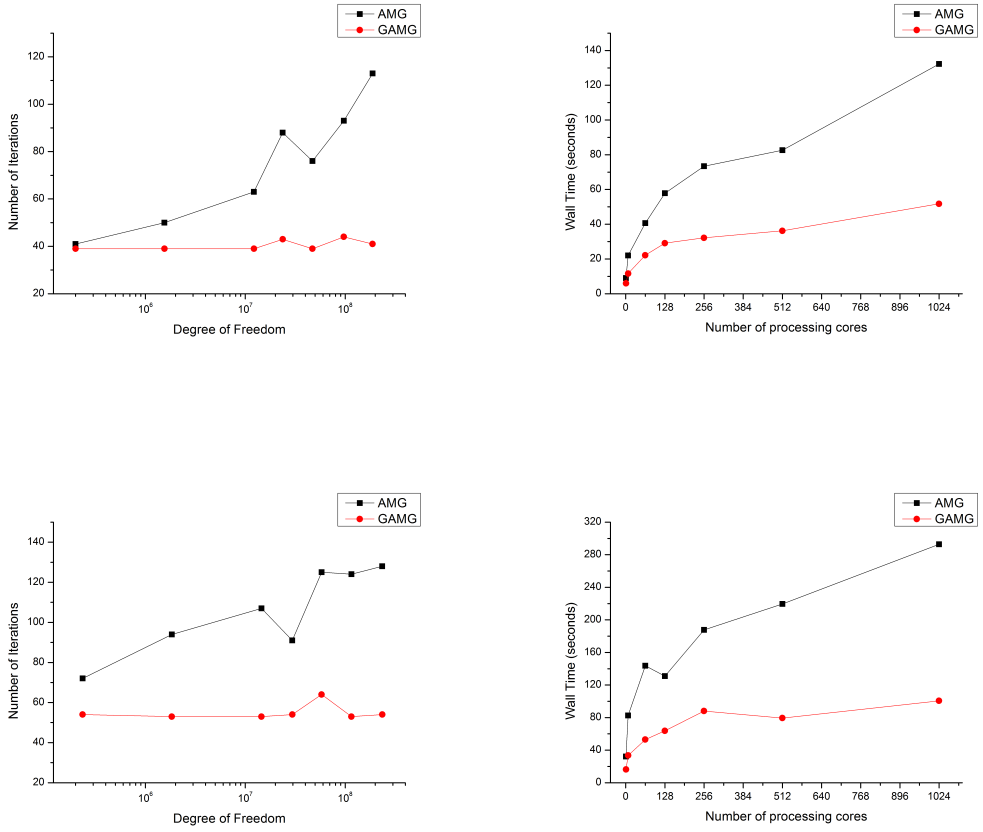

Difficulties in Simulating Non-Newtonian Fluids

1. There is a stability issue at high Weissenberg number regime.
2. FEM-formulation is done using Hood-Taylor mixed elements for which there is still a room to be improved in the efficiency of the Stokes solver.
3. Local solvers for the conformation tensor can be enhanced by employing the parallel technique.

Full nonlinear iterations can be GPU enhanced ! – with Wenjie Sha

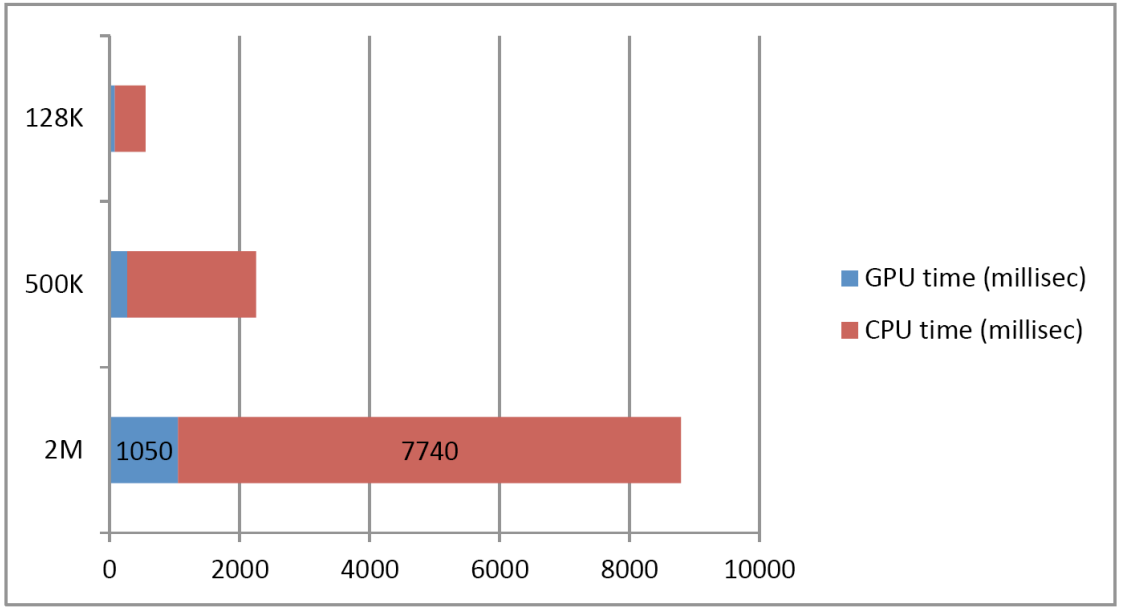

Figure: The test results of GPU implementation of FEM on unstructured grids with using element numbers of size 128K, 512K and 2M. We achieved about speed up of 7.4 times a sequential computation time.

Heterogeneous Computing : CPU + GPUs ongoing !

Conclusions

1. We introduced methods to handle non-Newtonian equations in a unified fashion and a stable manner
2. We provided new boundary conditions for diffusive models
3. We presented fast solvers for (time dependent) Stokes equation based on both preconditioned MINRes and GMRes and Augmented Uzawa Method combined with multigrid methods to handle the nearly singular equation that appear in the algorithms
4. Systematic Upscaling for Turbulent Flow (2D and 3D) – with A. Brandt and B. Diskin
5. Full Parallel Computing for non-Newtonian fluids is under way – with L. Wei and C. Zhang both at the Chinese Academy of Science

Thanks for your attention !

I would like to acknowlege supports from

- NSF-DMS 0915028 and AIP fund from Rutgers University.